Liquid interactions with porous media and the fate of toxic materials

Problem presented by

Simon Parker and James Nally

Defence Science and Technology Laboratory

Executive Summary

Toxic liquid chemicals released into the environment may pose an immediate risk to human health through contact or related vapour hazards. However, they can also interact with surfaces and remain in situ, potentially presenting a subsequent hazard. To improve understanding of the fate of these materials in different environments, the study group investigated interactions between liquid droplets and porous media across a range of different time scales.

Splashing and the subsequent re-entrainment of micro-droplets into the atmosphere was identified as one possible mechanism though which the area effect of a contamination could be significantly increased. The study group looked at experimentally determined splashing thresholds for droplet impacts with impermeable substrates, to determine initial predictions of whether or not a given droplet will splash. In cases where splashing occurs the droplet inertia is the most significant effect driving the initial phase of the liquid infiltration into a porous media and the study group developed a model to investigate this behaviour.

For longer time scales the study group determined that capillary suction played the most significant role in spreading the liquid within the porous medium. Models for the evolution of the partial saturation within a porous medium based on Richards' equation were investigated. Over even longer time scales evaporation converts the liquid back into a potentially hazardous vapour. The study group started to incorporate evaporation into models of liquid infiltration in a porous medium in order to describe this phenomenon. Recommendations for future theoretical, numerical and experimental modelling are also provided.

Report authors

Peter Hicks (University of Sheffield)
Andrew Crosby (University of Cambridge)
Duncan Hewitt (University of Cambridge)
Matt Hennessy (University of Oxford)
James Herterich (University of Oxford)
Iain Moyles (University of British Columbia)

Contributors

Abdulah Alzahrani (Heriot-Watt University)
Andrew Crosby (University of Cambridge)
Neil Deacon (University of East Anglia)
James Herterich (University of Oxford)
Matt Hennessy (University of Oxford)
Duncan Hewitt (University of Cambridge)
Peter Hicks (University of Sheffield)
Tania Khaleque (University of Oxford)
Andrew Lacey (Heriot-Watt University)
Georgina Lang (University of Oxford)
Iain Moyles (University of British Columbia)
Hillary Ockendon (University of Oxford)
John Ockendon (University of Oxford)
Emilian Părău (University of East Anglia)
Colin Please (University of Southampton)
Richard Purvis (University of East Anglia)
Moritz Reinhard (University of East Anglia)
Zimei Rong (University of Essex)
Julian Thompson (University of East Anglia)
Martin Walters (University of East Anglia)
Liyan Yu (University of Cambridge)
Agnieszka Zelerowicz (Polish Academy of Sciences)

Contents

1 Introduction

1.1 Background and scope

(1.1.1) Many toxic industrial chemicals and chemical warfare agents enter the environment in the form of liquid droplets. These liquid droplets can impact and subsequently interact with a wide range of different surfaces. If a droplet hits an impermeable surface, then it is comparatively easy to remove by cleaning the solid surface. However, if the solid is porous, then some of the liquid may enter the pore spaces of the solid, from where it is much harder to remove. Even after the remains of a liquid droplet have been cleaned from the surface of the solid, the liquid held within the pore spaces can escape back to the surface, though either liquid seepage or (after evaporation), in vapour form; potentially causing a hazard.

(1.1.2) The Defence Science and Technology Laboratory [DSTL] are keen to understanding how liquid droplets interact with porous surfaces in order to understand how droplets may enter the materials pore spaces and how long they persist inside them. A greater understanding of these processes will potentially help mitigate the long term hazards associated with the release of industrial chemicals and chemical warfare agents.

(1.1.3) Interactions between liquid droplets and porous media can have a multitude of different outcomes depending on the relative length scales associated with the droplet and the pore size. After discussion with DSTL, the study group focussed on problems in which the characteristic length scale of the droplet is typically much larger than the length scale of a pore, so that there is a well defined interface marking the edge of the porous media. It is with this surface that the droplet first makes contact. The study group noted that if the typical size of the droplets is equal to or is significant less than typical the pore size, then significantly different dynamics and interactions will result. Interactions in this regime where not investigated in the study group, but could include many interactions of interest to DSTL, such as the interaction tiny between aerosolized liquid droplets and porous surfaces.

(1.1.4) After discussion with DSTL the study group focussed on droplets with volumes between 0.1 and $10 \, \mu\text{L}$. These droplets have an equivalent range for their undisturbed diameters of between 0.29 and 1.34 mm. Droplet velocities upon contact with the porous media of up to $5 \, \text{m s}^{-1}$ were considered; an upper limit that is determined by the free-fall velocities of droplets under gravity released from rest within a room. It was noted that in the event of an explosive release of the liquid droplets, the impacts speeds with the porous media are likely to be significantly greater. The study group focused on three different liquids: Sarin, Sulphur Mustard and VX. Further properties of these substances are provided in Table 3.

(1.1.5)   The study group considered a range of different porous materials, but focussed specifically on interactions of droplets with sand and concrete. These two materials encompassed the range of porosities and permeabilities that were of interest to DSTL. Further details of the properties of these porous media are given in Table 4. The study group noted that sand is a granular material and that the impact of a liquid droplet may move individual grains and deform the interface of the sand. The consequences of the deformation of any of the porous media is not considered in this report.

(1.1.6)   One of the key problems considered by DSTL and the study group was to identify the different phases of a droplet impact and interaction with a porous media and to try an quantify the time scales over which the different types of interaction correspond to the dominant behaviour. To address this problem, this report describes the processes associated with droplet interactions with porous media in increasing time scales, starting with the initial droplet impact and splashing (or otherwise) in section 2. In sections 3 and 4 two different models are outlined, which describe the infiltration of a liquid droplet through the surface of a porous media and its subsequent evolution within the porous media. Finally, section 5 briefly describes possible approaches that could be used to model the longer time evaporation of the liquid within the pore spaces. Conclusions are drawn and recommendations for future work are made in section 6.

2   Droplet splashing upon impact with porous media

2.1   Droplet splashing upon impact with a flat impermeable plate

(2.1.1)   If a droplet splashes during an impact, then the generation of splash ejecta in the form of micro-droplets allows the material contained within a droplet to be entrained in the air and subsequently spread over a much larger area than if the droplet had not splashed on impact. Often these small micro-droplets can be carried in an airflow significant distances from the initial droplet impact site and greatly increasing the zone over which contamination occurs.

(2.1.2)   Theoretical and experimental investigations of droplet impacts onto porous media are very much in their infancy. High-speed photography has captured the impact of droplet into a granular powder [16], and this may provide some insight into the possible behaviours associated with impact with sand. However, further investigation of droplet impacts with porous substrates would be beneficial, not just for the problem presented by DSTL,

but also for a wide range of other important physical problems such as printing on clothes and pesticide uptake in soils.

(2.1.3)   Research into droplet impacts with impermeable substrates is more established, and many theoretical and experimental studies have investigated this problem. If a droplet has sufficient inertia when it impacts an impermeable substrate, then it initially forms a thin liquid jets that runs radially out from the impact site, across the surface of the substrate. Following the definition of Mundo *et al.* (1995) [18], a splash occurs when these splash jets separate from the substrate and break up in the air to form micro-droplets. However, a full description of the mechanism detailing all the factors responsible for the lift off of a splash jet is unavailable at this time.

(2.1.4)   In the absence of theoretical and experimental results detailing droplet impacts with porous surfaces it makes sense to ask what are the conditions which lead to splashing in droplet impacts with an impermeable substrate? Subsequently the differences that may result from a porous substrate can be evaluated. Mundo *et al.* (1995) [18] experimentally determined that the onset of splashing for droplet impacts with flat impermeable horizontal plates is given by

$$\text{Oh Re}^{5/4} > 57.7 \tag{1}$$

where the Ohnesorge and Reynolds numbers are given by

$$\text{Oh} = \frac{\mu}{\sqrt{\rho D \sigma}}, \quad \text{and} \quad \text{Re} = \frac{\rho V D}{\mu}, \tag{2}$$

respectively. The Ohnesorge number relates the viscous forces to inertial and surface tension forces, while the Reynolds number is a measure of the ratio of inertial forces to viscous forces on the droplet. These quantities are based on a droplet of diameter D, impact velocity V, density ρ, viscosity μ and surface tension σ.

(2.1.5)   Figures 1, 2 and 3 show the splashing threshold (1) for droplets of Sarin, sulphur mustard and VX, respectively. To give an indication of droplet impact speeds, the impact speeds for spheres of equivalent diameter released from rest are also plotted for release heights of 0.1, 0.2, 0.3, 0.4 and 0.5 metres above the impact site. This shows that for very small droplets released close to the ground surface will not splash, but for larger droplets (corresponding to the majority of the parameter range of interest to DSTL), splashing will occur upon impact with an impermeable solid. As the viscosity of the fluid increases, the propensity of a droplet to splash reduces, with Sarin (the least viscous fluid), being most likely to splash, followed by sulphur mustard with VX (the most viscous liquid), being least likely to splash. However, even with VX, the largest droplets of interest to DSTL will splash when released from heights over 0.1 m.
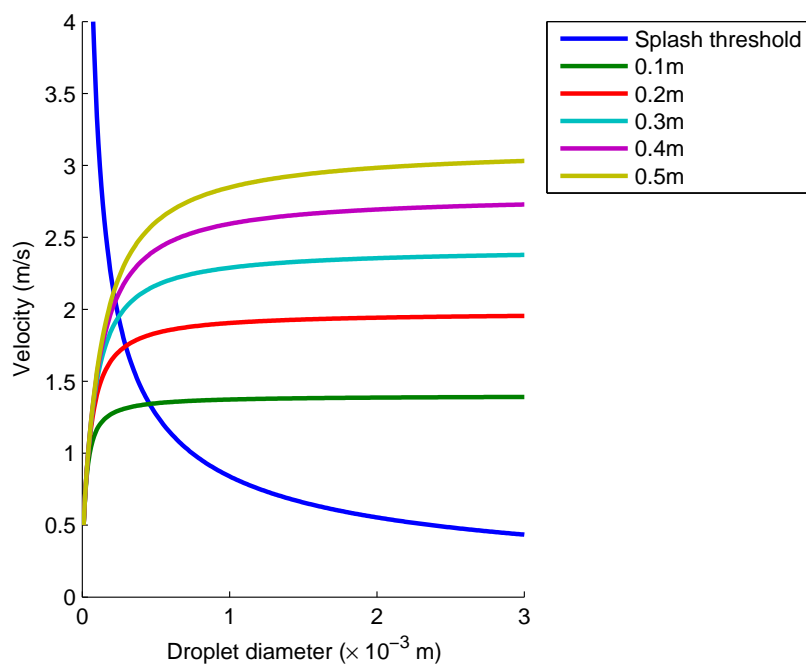
**Figure 1:** A regime diagram showing the experimentally determined condition for the onset of splashing for a droplet of Sarin, with splashing predicted for impacts above the solid blue line. Also shown are the impact speeds for droplets released from rest from 0.1, 0.2, 0.3, 0.4 and 0.5 m above the substrate.
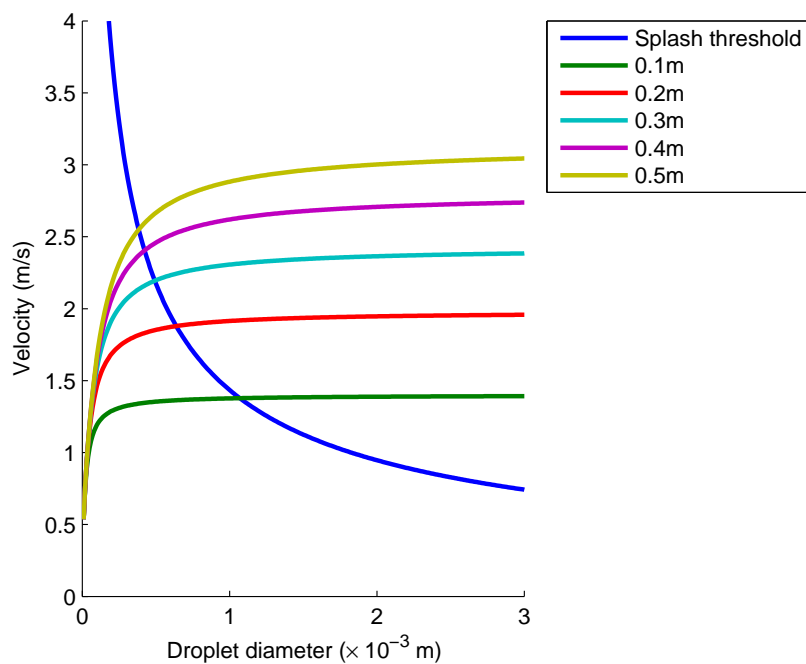

Figure 2: As figure 1, but showing the splashing threshold and impact speeds for droplets of sulphur mustard.
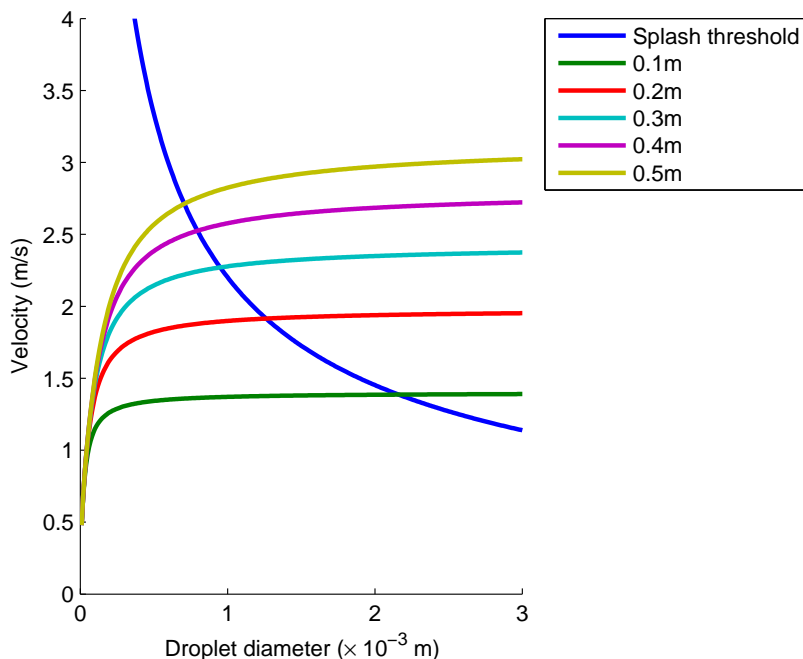
Figure 3: As figure 1, but showing the splashing threshold and impact speeds for droplets of VX.

(2.1.6)   The experimentally determined relationship (1) is only valid for droplet impacts close to atmospheric pressure and it is known that at lower ambient gas pressures the tendency for a droplet to splash is suppressed [27], while small changes in the roughness of the solid surface are also critical for triggering splashing [14]. However, equation (1) does suggest that for droplets of the size that is of interest to DSTL, that splashing will occur upon impact with a rigid impermeable substrate. The next question to consider is how does a porous substrate change this conclusion.

2.2   Initial stages of a droplet impact on a porous medium

(2.2.1)   Little work has been done on the effect of roughness and surface porosity on splashing. More experimental data is needed to determine the splash threshold condition for droplets impacting a porous media. In impacts with a porous medium, additional factors over and above those associated with impact with a flat impermeable substrate will effect the outcome. These additional effects including the surface roughness, porosity and permeability of the porous medium.

(2.2.2)   For much of the parameter range of interest, the initial stages of a droplet impact is dominated by inertia of the droplet. The effect of viscosity, surface tension and gravity on the droplet motion can be neglected if the

Reynolds number, the Weber number and the Froude number given by

$$\text{Re} = \frac{\rho V D}{\mu} = 3170.0, \tag{3a}$$

$$\text{We} = \frac{\rho V^2 D}{\sigma} = 339.0, \tag{3b}$$

$$\text{Fr} = \frac{V^2}{gD} = 204.0, \tag{3c}$$

respectively, are all much greater than one. The numbers shown correspond to a droplet of Sarin with an undisturbed diameter $D = 1\,\text{mm}$ and an impact speed $V = 2\,\text{m s}^{-1}$, and indicate that inertia dominates the initial stages of the droplet impact and effects due to viscosity, surface tension and gravity can be neglected at least initially. After this initial stage of the impact, the effect of viscosity and surface tension will become more significant. However, it is of interest to consider this initial inertia dominated phase of a droplet impact with a porous medium as it determines the splashing behaviour. The corresponding Ohnesorge number for these droplet parameters $\text{Oh} = 0.006$, while from equation (1), the splashing criterion $\text{Oh Re}^{5/4} = 138.3$ indicating splashing is to be expected if this droplet impacts a rigid impermeable surface.
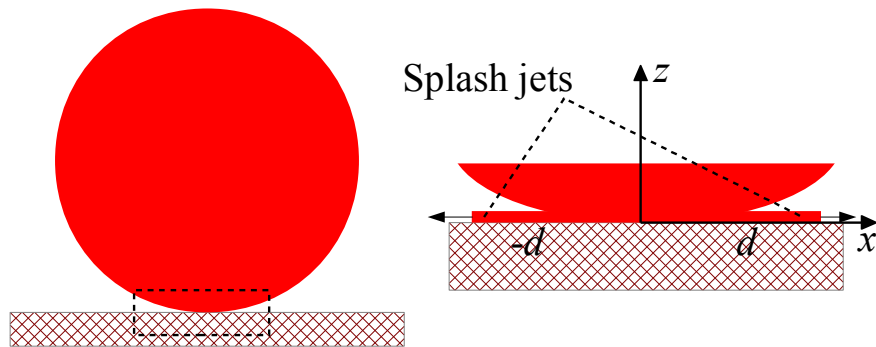
Figure 4: An idealized liquid droplet impacting on a solid surface, showing the formation of splash jets running over the solid surface.

(2.2.3) In a small region surrounding the point where (an idealized two dimensional), droplet initially touches down on a porous medium, the velocity potential associated with the fluid ϕ, can be modelled by a mixed boundary value problem with the form

$$\begin{cases} \nabla^2 \phi(x,\, z,\, t) = 0, & \\ \phi_z(x,\, 0,\, t) = -1 + V(p), & |x| < d(t), \\ \phi(x,\, 0,\, t) = 0, & |x| > d(t), \\ \phi \to 0, & x^2 + z^2 \to \infty, \end{cases} \tag{4}$$

where the penetration velocity of liquid into the porous media is denoted $V(p)$. Here we consider a penetration velocity with the form

$$V(p) = V_{drop}(x,\,0,\,t) - V_{body}(x,\,0,\,t) = \alpha p_0(t)\,, \qquad (5)$$

where $p_0(t) = p(0,\,0,\,t)$, and α is proportional to the porosity (see figure 4). The region $|x| < d(t)$ is called the contact patch inside which the body of the droplet is in contact with the substrate, while outside the contact patch only liquid jets are in contact with substrate. This problem is called a mixed boundary value problem because different boundary conditions are applied inside and outside the contact patch region.

(2.2.4) Mixed boundary value problems such as this have previously been used to model the initial stages of blunt impermeable body impact with water [12, 20], of which droplet impact with a flat impermeable substrate is just a special case. Extensions of the basic theory covering droplet impacts have included impacts with rough impermeable substrates [8], and thin liquid layers [22, 11]. Mixed boundary value problems have also been used to model the entry of a porous wedge into a much larger body of liquid [17, 13]. A porous wedge has a sharp point where the body initially enters the liquid domain and prior to the study group no attempt has been made to model the impact of a liquid with a blunt porous body (such as the impact of an initially circular droplet with a porous substrate).

(2.2.5) The solution to the mixed boundary value problem (4) is given by

$$p(x,\,0,\,t) = -\alpha \dot{p}_0 \sqrt{d^2 - x^2} - \frac{\dot{d}}{2}\left(-1 + \alpha p_0\right)\left(\sqrt{\frac{d-x}{x+d}} - \sqrt{\frac{x+d}{d-x}}\right), \quad (6)$$

and in particular the pressure below the centre point of the droplet is given by

$$p_0 = -\alpha \dot{p}_0 d - \alpha p_0 \dot{d} + \dot{d}, \quad \text{for} \ \ x = 0. \qquad (7)$$

(2.2.6) The limits of the contact patch $d(t)$, are determined by *Wagner's condition*, which states that the elevation of the free surface must equal the elevation of the solid body at the contact point. For an impermeable body ($\alpha = 0$) the contact patch grows like $d(t) = \sqrt{2t}$ [20], while for a completely permeable body the droplet does not deform and geometrical considerations imply $d(t) = \sqrt{t}$.

(2.2.7) This suggest an ansatz for small time t, with the form:

$$d(t) = a\sqrt{t} \ \ \text{for} \ \ a \in \left[1,\,\sqrt{2}\right], \qquad (8a)$$

$$p_0(t) = b + ct^\lambda. \qquad (8b)$$

A solution to this problem is obtained with $a = 1$, $b = \alpha^{-1}$, $c = -\alpha^{-2}$ and $\lambda = \frac{1}{2}$. For small time this solution has the form

$$d(t) = \sqrt{t} + \text{positive higher order correction};\tag{9a}$$

$$p_0(t) = \frac{1}{\alpha} - \frac{\sqrt{t}}{\alpha^2},\tag{9b}$$

while the penetration depth into the porous medium is given by

$$H = \alpha \int_0^t p_0(\tau) \, \mathrm{d}\tau = t - \frac{2t^{3/2}}{3\alpha}.\tag{9c}$$

Penetration depths for small α (an impermeable substrate), $\alpha = 1$ and α large (a fully permeable substrate), are sketched in figure 5 and show that the depth of the initial inertia driven penetration increases with the porosity of the medium.
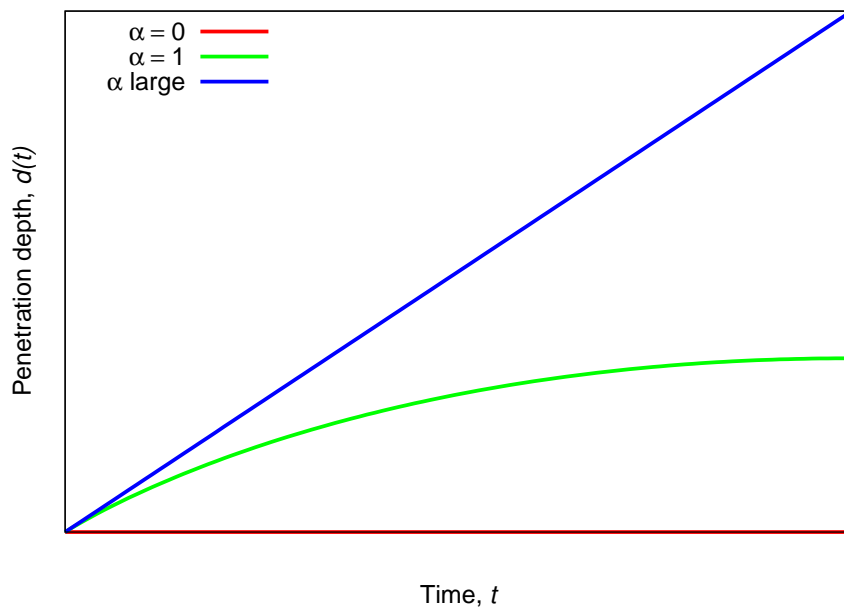
Figure 5: Idealized penetration depths as a function of the parameter α.

(2.2.8) These preliminary results suggest that the initial impact pressure in a droplet impact with a porous substrate is less than the pressure in an impact with an impermeable body, from which we tentatively postulate that the splash jets running over the substrate surface may have reduced velocity compared to their counterparts created in impacts with impermeable substrates. Additionally the size of the wetted contact patch decreases as the porosity rises, inertia is responsible for forcing liquid into the pore spaces and the penetration depth is dependent upon the porosity. The study group believes that a mixed boundary value problem like this is a

good way of analysing the inertia dominated phase of a droplet impact and also of verifying the initial predictions from numerical simulations of droplet impact. The modelling herein assumes the infiltration velocity throughout the contact patch is determined just by the pressure below the centre point of the droplet (see equation (5)). Given more time a coupled problem in which the infiltration velocity is determined by the local pressure at each point, i.e.

$$V(p) = V_{drop}(x,\, 0,\, t) - V_{body}(x,\, 0,\, t) = \alpha p(x,\, 0,\, t)\,, \qquad (10)$$

provides an excellent candidate for further study.

(2.2.9)   These results qualitatively support the full numerical calculations Reis *et al.* [23, 24], who show the horizontal spreading of a droplet is reduced and the penetration depth increases as the porosity of the substrate rises. The study group notes that although these results and existing numerical calculations [23, 24] predict the splash jets running over the surface of a porous substrate will have lower velocity in an impact with a porous medium relative to an impermeable substrate, this does not necessarily mean the likelihood of these splash jets detaching from the surfaces is reduced. On the contrary, small changes in surface roughness (which might be expected on the surface of a porous substrate), more readily trigger splash jet lift off [14]. The competing effects of porosity and surface roughness on droplet splashing are a long way from being fully understood and the study group suggests further theoretical, numerical and experimental investigations are required to better understand these important phenomena.

3   Two zone models of droplet infiltration into porous media

3.1   1D Darcy model of droplet infiltration

(3.1.1)   After the inertial impact, the droplet will continue to be drawn into the porous medium by three processes: gravity acting on the whole droplet, surface tension acting at the top surface of the drop, and capillary suction acting at the interface between the droplet and the unsaturated porous medium.

(3.1.2)   Capillary suction arises from surface tension effects between the porous medium and the liquid, which act to draw fluid into the pore spaces. Surface tension σ causes a pressure drop across the interface, P_c, which can be estimated [6] as

$$P_c = \frac{2\sigma \cos\theta}{b}, \qquad (11)$$

where θ is the contact angle for that particular liquid-solid pairing, and b is a characteristic pore size. The value of b is typically measured experimentally using mercury porosimetry [10].

(3.1.3) For the liquids of interest here σ is typically $0.03\ \mathrm{Pa\,m^{-1}}$. Assuming a contact angle of $45°$, and pore-sizes in the range $0.5\ \mu\mathrm{m} - 50\ \mu\mathrm{m}$, suggests that typical values for the capillary suction pressure are in the range $10^3 - 10^5$ Pa. These values are sufficiently large that the effect of capillary suction is likely to dominate the effects of gravity and surface tension at the droplet-air interface in the absorption process. Therefore, for the rest of this section, we assume that the flow is driven by capillary suction alone.

(3.1.4) The effect of capillary suction is most simply modelled by considering a one-dimensional flow where we assume that a sharp front exists between a fully saturated region and an unsaturated region (Figure 6). The flow in the fully saturated region can be modelled by Darcy's law, and is driven by the pressure drop P_c across the advancing saturation front. Such a model has previously been considered in the literature [1, 6].
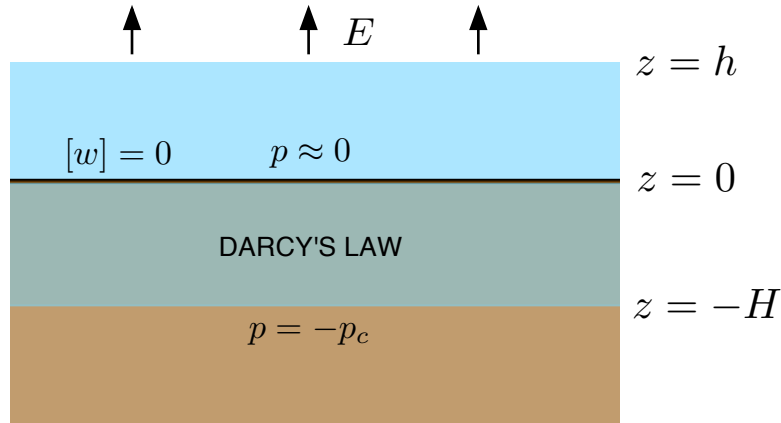
Figure 6: 1D model of droplet absorption due to capillary suction. There is assumed to be a sharp front between a fully saturated region, of height H, and the dry porous medium beneath. The height of liquid above the porous medium is h.

(3.1.5) Darcy's law applied to the fully saturated region of depth H gives an expression for the average fluid velocity within the medium, w, and, consequently, for the rate at which the front of the saturated region advances into the porous medium

$$\phi\frac{dH}{dt} = w = \frac{k}{\mu}\frac{P_c}{H}. \tag{12}$$

In this expression μ is the viscosity of the fluid, ϕ the porosity of the porous

medium and k the permeability of the porous medium; all of which we assume to be constant.

(3.1.6) Solving this differential equation gives an expression for the rate at which the front propagates into the porous substrate

$$\frac{dH}{dt} = \sqrt{\frac{kP_c}{2\mu\phi t}},\tag{13}$$

and an expression for how the depth of the front evolves with time

$$H = \sqrt{\frac{2kP_c t}{\mu\phi}}.\tag{14}$$

(3.1.7) The height h of the fluid layer above the surface is initially h_0, and evolves according to

$$h = h_0 - \sqrt{\frac{2kP_c\phi}{\mu}}t^{1/2} - Et,\tag{15}$$

where we have also included the effect of an evaporative loss from the surface of the liquid, modelled as a constant velocity E.

(3.1.8) We note that, in the absence of evaporation ($E = 0$), the liquid interface has penetrated a distance h_0/ϕ into the porous medium by the time that the droplet is fully absorbed.

(3.1.9) Under this simple model, the propagation of the fluid interface stops as soon as the droplet is fully absorbed into the porous medium, at which point the capillary suction at the liquid interface within the porous medium is balanced by a similar suction acting in the opposite direction at the top surface. Investigation of the later time evolution of the droplet within the porous medium requires a more detailed model able to capture the behaviour of a semi-saturated region.

3.2 Time scales for droplet absorption

(3.2.1) This simple one-dimensional model gives us a prediction for the time scale over which the drop will be fully absorbed into the porous medium

$$T_{\text{drainage}} = \frac{h_0^2\mu}{2kP_c\phi} = \frac{h_0^2\mu b}{4k\phi\sigma\cos\theta}.\tag{16}$$

In this expression k, ϕ and b are properties of the solid, and as such only need to be measured once for each solid substrate. Similarly μ and σ are properties of the liquid only. The only parameter that depends on the particular liquid-solid substrate pairing is the contact angle θ, which can be easily measured experimentally.

(3.2.2) This drainage time scale can vary drastically between different porous media (e.g. sands with different grain sizes) because b and k both vary over multiple orders of magnitude. The time scales are discussed further in section 4.4.

3.3 Richards' equation

(3.3.1) A more realistic model for the evolution of the liquid within the porous medium is obtained by allowing for the presence of a semi-saturated region within the porous medium, in which only a fraction $0 \leq S \leq 1$ of the pore space is filled with liquid.

(3.3.2) Flow in a semi-saturated porous medium is governed by Richards' equation [25]

$$\phi \frac{\partial S}{\partial t} = \nabla \cdot (D_0 D(S) \nabla S),$$ (17)

where $D_0 D(S)$ is the diffusivity of liquid at saturation S within the porous medium. D_0 can be expressed in terms of liquid and solid properties as $D_0 = ckP_c/\mu$ for some dimensionless constant c (which can be absorbed into the definition of $D(S)$).
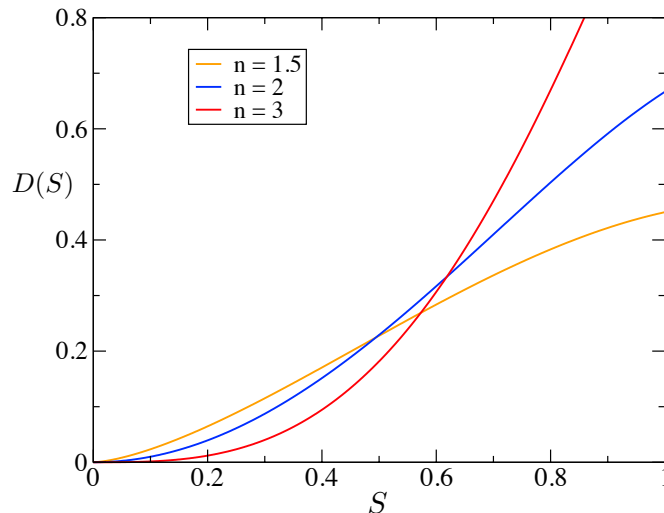
Figure 7: Form of $D(S)$ as given by equation (18), for $n = 1.5$, 2 and 3.

(3.3.3) The form of the dimensionless function $D(S)$ (and the value of c) depend on the structure of the porous medium and on the contact angle θ. The behaviour of $D(S)$ for small values of S determines whether a sharp front forms between the semi-saturated region and the dry region below, and also determines the rate at which the liquid propagates through the porous medium at long times. We choose to work with

$$D(S) = \frac{n}{2} S^n \left(1 - \frac{S^n}{n+1}\right),$$ (18)

12

which has a completely general power-law behaviour for small S. The behaviour of $D(S)$ for large S is less realistic, but does allow for analytic solution of the equations. The variations of $D(S)$ with S, for a several typical values of n associated with porous media, are shown in Figure 7.

3.4 1D Similarity solution - short time

(3.4.1)   We again consider a one dimensional model for the evolution of the droplet within the porous medium. However, now we replace the fully saturated region from our earlier model (Figure 6) with a partially saturated region where flow is governed by the one dimensional Richards' equation

$$\phi\frac{\partial S}{\partial t} = \frac{\partial}{\partial z}\left(D_0 D(S)\frac{\partial S}{\partial z}\right). \tag{19}$$

(3.4.2)   While the drop remains on the surface, the boundary condition at the top boundary of the porous medium is $S(0,t) = 1$, i.e. the top of the porous medium is fully saturated.

(3.4.3)   The subsequent evolution of S can be calculated analytically [26] and exhibits a self-similar behaviour (c.f. diffusion of heat in a metal bar heated at one end). The evolution is given by

$$S(\eta) = (1 - \eta)^{1/n}, \tag{20}$$

where

$$\eta \equiv \left(\frac{\phi}{D_0}\right)^{1/2}\frac{x}{t^{1/2}}. \tag{21}$$

(3.4.4)   The solution forms a sharp front at $\eta = 1$ between the partially-saturated porous medium and the dry porous medium below. The shape of the solution, for $n = 2$, is shown in Figure 8. The depth of the front grows as $(D_0 t)^{1/2}$; this $t^{1/2}$ growth is completely independent of the choice of $D(S)$, and agrees with our earlier model based on a fully saturated region governed by Darcy's law.

(3.4.5)   This solution continues to be valid until the droplet is fully absorbed from the surface. The time taken for absorption depends on the exact form of $D(S)$, but otherwise has the same functional depedence on liquid and solid parameters as the earlier Darcy model.

3.5 1D Similarity solution - long time

(3.5.1)   Once the droplet has been fully absorbed, a boundary condition of $S(0,t) = 1$ at the surface of the porous medium is no longer appropriate. Instead, in
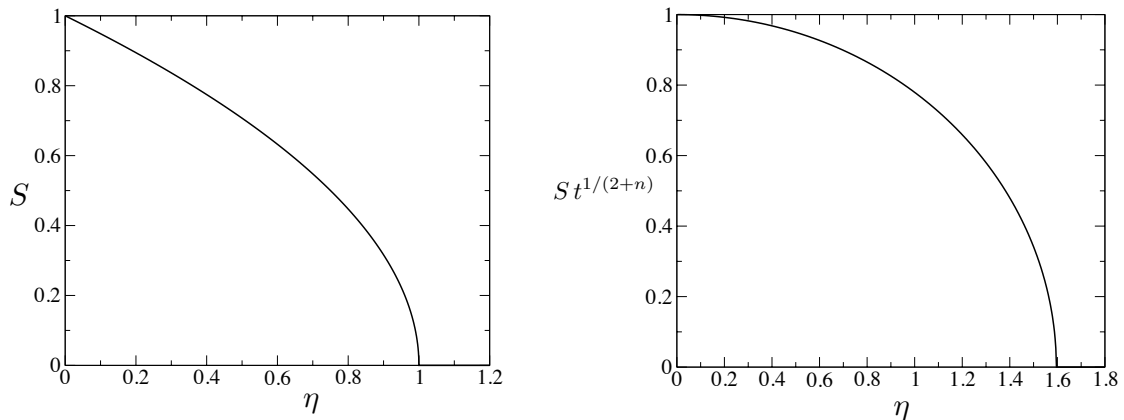
Figure 8: Shapes of self-similar solutions for the case $n = 2$. Short-time solution when droplet is not fully absorbed (left) and long-time solution after droplet has been absorbed (right).

the absence of any evaporation from the surface, there should be a no-flux constraint

$$- D_0 D(S) \frac{\partial S}{\partial z} = 0. \tag{22}$$

This is equivalent to requiring that the total volume of liquid within the porous medium remains constant

$$\int_0^{z_{\text{front}}} \phi S(z, t) \, \mathrm{d}z = h_0. \tag{23}$$

(3.5.2) At long times, we can make a small S approximation to the diffusivity

$$D(S) \approx \frac{n}{2} S^n \tag{24}$$

and it is again possible to find a self-similar solution

$$S(z, t) \equiv \frac{h_0}{\phi} \frac{f(\eta)}{z}, \tag{25}$$

where

$$f(\eta) = \eta \left(c(n) - \frac{\eta^2}{n + 2} \right)^{1/n} \quad \text{and} \quad \eta \equiv \left(\frac{\phi^{1+n}}{D_0 h_0^n} \right)^{1/(2+n)} \frac{z}{t^{1/(2+n)}}. \tag{26}$$

The constant $c(n)$ is determined by the constraint

$$\int_0^{\eta_{\text{front}}} f(\eta)/\eta \, \mathrm{d}\eta = 1. \tag{27}$$

(3.5.3) There is still a sharp front between the semi-saturated porous medium and the dry porous medium beneath, but the rate of spread has slowed, from the earlier $t^{1/2}$ while the droplet was on the surface, to $t^{1/(2+n)}$. Importantly, the long time evolution rate of the front depends on n and, consequently, on the form of $D(S)$.

14
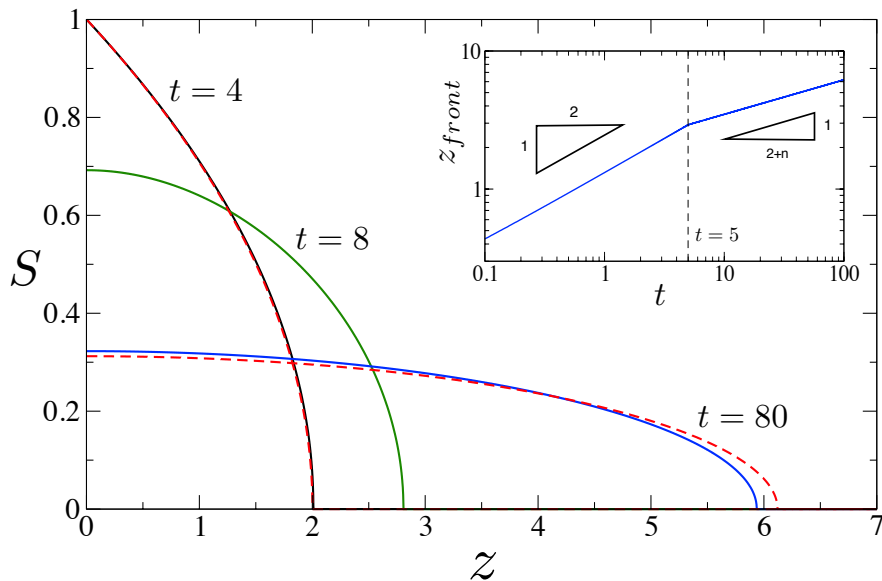
Figure 9: Numerical solution of Richards' equation with $n = 2$ (solid lines). The drop is fully absorbed into the porous medium at $t = 5$. Short and long time similarity solutions are also shown (dashed lines) and are in good agreement with the full numerical solution. The spreading of the front is observed to slow from $t^{1/2}$ to $t^{1/4}$ once the droplet is fully absorbed (inset).

(3.5.4)   The one dimensional Richards' equation can be solved numerically in order to verify to two self-similar solutions. Such a numerical evolution for the case $n = 2$ is shown in Figure 9. While the droplet is on the surface, there is good agreement with the first similarity solution. Then, after a transient transition period, there is good agreement with the second similarity solution.

3.6   3D Similarity solution - long time

(3.6.1)   For a single droplet, a one-dimensional model is not particularly realistic at long times, since the droplet can be expected to spread out laterally as well as vertically within the porous medium. Instead, at long times, the droplet can be viewed as a point source release of a finite quantity of fluid, leading to a radially symmetric solution $S(r, t)$ of Richards' equation

$$\phi \frac{\partial S}{\partial t} = \frac{1}{r^2} \frac{\partial}{\partial r} \left(r^2 D_0 D(S) \frac{\partial S}{\partial r} \right), \tag{28}$$

which satisfies a fixed volume (V_0) constraint

$$\int_0^{r_{\text{front}}} \phi S(r, t) 4\pi r^2 \, \mathrm{d}r = V_0. \tag{29}$$

(3.6.2)   Making the small S diffusivity approximation

$$D(S) \approx \frac{n}{2} S^n \tag{30}$$

15

again allows for a self-similar solution

$$S(r,t) \equiv \frac{V_0}{4\pi\phi}\frac{g(\eta)}{r^3}. \tag{31}$$

where

$$g(\eta) = \eta^3 \left(d(n) - \frac{\eta^2}{3n+2}\right)^{1/n} \quad \text{and} \quad \eta \equiv \left(\frac{\phi^{1+n}(4\pi)^n}{D_0 V_0^n}\right)^{1/(2+3n)} \frac{z}{t^{1/(2+3n)}}. \tag{32}$$

The constant $d(n)$ is determined by the constraint

$$\int_0^{\eta_{\text{front}}} g(\eta)/\eta \, \mathrm{d}\eta = 1. \tag{33}$$

(3.6.3)   The main difference, when compared to the earlier one-dimensional solution, is that the spreading rate in three dimensions is $t^{1/(2+3n)}$, which is slower than the $t^{1/(2+n)}$ spreading rate of the one-dimensional solution.

4   Three zone models of droplet infiltration into porous media

4.1   Three Zone Model

(4.1.1)   A two-region model insinuates a passive diffusion mechanism in the porous media because the only reason pores fill is due to the strong capillary pressure between the heavily saturated droplet and the porous media which is vacuous in liquid. However, if a droplet of liquid impacts a porous medium with a sufficiently large force or pressure, then without consideration of porous pressure-driven flows, the impact of the liquid on the porous surface will fill some of the pores immediately to full saturation (as demonstrated in section 2.2). For this reason, one might expect the creation of a thin, fully-saturated region near the surface of the porous medium; a third zone which separates the liquid droplet from the passive porous diffusion layer. If this is indeed the case, then capillary suction from the unsaturated region will draw fluid from the fully-saturated region and not from the droplet. The dominant mechanism for driving fluid from the droplet into the porous medium is then expected to be pressure gradients between the droplet and the fully-saturated region. The existence of this fully-saturated region will be explored by extending the above two-zone model to include this region.

4.2   1D Model: Governing equations

(4.2.1)   We consider a simplified one-dimensional model of this three zone structure as depicted in Figure 10. The pressure, velocity, and time variables

16

are non-dimensionalized using the respective scales

$$P = P_c, \quad W = \frac{kP_c}{\mu H}, \quad T = \frac{H\phi}{W}, \tag{34}$$

where P_c is a reference capillary pressure, H is the initial height of the droplet, W is the fluid velocity, ρ is the density of the droplet, k and ϕ are the permeability and porosity of the porous medium, respectively, and g is the acceleration due to gravity. Typical values are presented in Table 1.

Air

$z = h_1(t)$

Fluid

$z = 0$

Fully-saturated region

$z = h_2(t)$

Partially-saturated region

$z = h_3(t)$

Unsaturated porous media
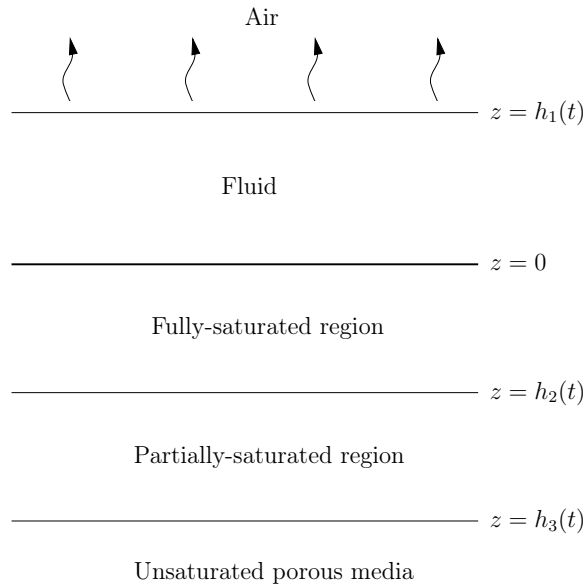
Figure 10: When droplet impact is considered, a fully saturated middle layer may appear which separates the droplet from the porous diffusion layer. The capillary pressure then has the role of drawing this saturated layer further into the soil. The voids left in the saturated region from such a mechanism are resaturated by liquid from the droplet.

(4.2.2) In the fluid region above the porous medium, *i.e.*, the droplet, we consider the Navier-Stokes equations. The one-dimensional dimensionless equations read

$$\mathrm{Re}\left(\frac{1}{\phi}\frac{\partial w}{\partial t} + w\frac{\partial w}{\partial z}\right) = -\frac{1}{\mathrm{Da}}\frac{\partial p}{\partial z} + \frac{\partial^2 w}{\partial z^2} - \frac{1}{\mathrm{Da}}G, \tag{35}$$

$$\frac{\partial w}{\partial z} = 0. \tag{36}$$

where

$$\mathrm{Re} = \frac{\rho W H}{\mu}, \quad \mathrm{Da} = \frac{k}{H^2}, \quad G = \frac{\rho g H}{P_c}, \tag{37}$$

are the Reynolds number, the Darcy number, and an effective gravity force, respectively. Values for these non-dimensional numbers are presented in Table 1.

Table 1: Relevant parameter values for the three-zone mode. Parameter values come from either [15], equation (37), equation (34), or are provided by DSTL.

.

Parameter	Value	Description
H	1×10^{-3}m	Height of droplet
k	1×10^{-11}m^2	Reference permeability
ϕ	0.40	Porosity
μ	1×10^{-2}Pas	Reference fluid viscosity
ρ	1×10^3kg/m^3	Reference fluid density
E	1×10^{-1}kg/m^2/s	Evaporation coefficient
γ	1×10^{-2}N/m	Liquid-air surface tension coefficient
P_c	1×10^3Pa	Reference capillary pressure
g	10N/kg	Earth gravitational constant
W	1×10^{-3}m/s	Effective porous velocity
Re	1×10^{-1}	Reynolds number
Da	1×10^{-5}	Darcy number
G	1×10^{-2}	Gravity number

(4.2.3)   In the fully-saturated porous medium region we consider pure Darcy flow with a constant permeability. For this reason we will refer to this fully-saturated region as the Darcy region. The one-dimensional dimensionless equations read

$$\bar{w}_d = -\frac{\partial \bar{p}_d}{\partial z} + G, \tag{38}$$

$$\frac{\partial \bar{w}_d}{\partial z} = 0. \tag{39}$$

(4.2.4)   Finally, in the partially-saturated region, we again consider Richards' equations and assume a Darcy-like fluid velocity where the pressure in this region, $\bar{p}_s$, is prescribed (this will be elaborated on below). In particular, we have

$$\frac{\partial S}{\partial t} = \frac{\partial}{\partial z}\left(D(S)\frac{\partial S}{\partial z} - \kappa(S)G\right), \tag{40}$$

$$\bar{p}_s = -j(S), \tag{41}$$

$$\bar{w}_s = -D(S)\frac{\partial S}{\partial z} + \kappa(S)G, \tag{42}$$

where $\kappa(S)$ is the saturation dependent permeability, $D(S)$ is the dimensionless diffusivity of the liquid as a function of the saturation S and $j(S)$ is the saturation-dependent capillary pressure. This functional dependence may make the equations highly nonlinear.

18

4.3 Choosing the diffusivity

(4.3.1) To understand physical modelling of $D(S)$, we look at a non-dimensional saturation-dependent version of Darcy's Law,

$$\bar{w}_s = -\kappa(S)\left(\frac{\partial \bar{p}_s}{\partial z} - G\right),$$

where $\bar{p}_s = -j(S)$ is again, the capillary pressure in the porous medium. Upon substitution we get

$$\bar{w}_s = \kappa(S)j'(S)\frac{\partial S}{\partial z} + \kappa(S)G,$$

with prime in this context being a derivative with respect to S. Now by the continuity equation we have

$$\frac{\partial S}{\partial t} = -\frac{\partial \bar{w}_s}{\partial z} = -\frac{\partial}{\partial z}\left(\kappa(S)j'(s)\frac{\partial S}{\partial z} + \kappa(S)G\right).$$

To place this in the form of Richards' equation, we define the effective diffusivity as

$$D(S) = -\kappa(S)j'(S).$$

Therefore, an accurate model of the diffusivity is achieved by an accurate construction of the permeability and capillary pressure as they depend on S. When a region is fully saturated, the constituents should move via Darcy's law and so the permeability should be constant (non-dimensionally $\kappa(1) = 1$). Conversely, when the region is void, there should be no natural motion of the particles and hence $\kappa(0) = 0$ [15]. For this reason, much of the literature and engineering use a power law fit for permeability known as a Corey-type [4, 5]. We follow this scheme and take $\kappa(S) = S^3$.

(4.3.2) There are two important physical mechanisms when constructing the capillary pressure $j(S)$. Firstly, when the saturation goes to zero, there is an infinite suction pressure and so we need $j(S)$ to diverge there. Secondly, when the region is fully saturated there are no longer any surface tension effects that would act to fill the pores (since they already are completely filled) so the capillary pressure must vanish. Therefore, capillary pressure models usually take the form, $j(S) = (1 - S^\alpha)S^{-1/\alpha}$ with $\alpha > 0$ [15]. Without loss of generality, we take $\alpha = 4$ to represent a typical geophysical porous medium. We differentiate our capillary pressure and multiply it by our permeability to get,

$$D(S) = \frac{1}{4}S^{7/4}\left(1 + 15S^4\right). \tag{43}$$

4.4 1D Model: Boundary conditions

(4.4.1) On the liquid-air boundary $z = h_1(t)$, the kinematic boundary condition relates the motion of $h_1(t)$ to the flow into the porous medium and the evaporation of the droplet into the air. The dynamic boundary condition is continuity of pressure. The dimensionless kinematic and dynamic boundary conditions read

$$\frac{\mathrm{d}h_1}{\mathrm{d}t} = \phi w - \frac{T_{\mathrm{sat}}}{T_{\mathrm{evap}}}, \tag{44}$$

$$p = p_{\mathrm{top}}, \tag{45}$$

where

$$T_{\mathrm{sat}} = \frac{\mu \phi H^2}{P_c k}, \quad T_{\mathrm{evap}} = \frac{\rho H}{E}, \tag{46}$$

are dimensionless time scales for saturation into the porous medium and vapourization into the air. These time scales are equivalent to the ones derived in the two-region model. The pressure p_{top} is the pressure at the liquid-air boundary. This can be taken to be atmospheric pressure or, in a very simplified case, a combination of atmospheric pressure and an impact pressure resulting from the droplet landing on the porous medium. It is this pressure which represents the impact force of the droplet leading to the creation of a three-zone model.

(4.4.2) In high porosity and permeability materials such as sand, the time scale T_{sat} associated with the absorption of a chemical weapons agent is much shorter than the time scale associated with evaporation T_{evap}. Consequently for droplets impacting sand, the liquid will be absorbed before it has a chance to evaporate. Conversely for less porous and permeable materials such as concrete the time scales associate with absorption and evaporation can be of the same size, indicating that a significant proportion of a droplet may evaporate before infiltration.

(4.4.3) On the liquid-substrate boundary $z = 0$ there is continuity of pressure and velocity

$$p = \bar{p}_d, \tag{47}$$

$$w = \bar{w}_d. \tag{48}$$

On the fully-partially saturated boundary $z = h_2(t)$, the dynamic boundary condition is continuity of pressure and the kinematic boundary condition states that the boundary advances at a rate relative to the velocities of the fluid in the fully and partially saturated regions

$$\bar{p}_d = \bar{p}_s, \tag{49}$$

$$\frac{\mathrm{d}h_2}{\mathrm{d}t} = \bar{w}_d - \bar{w}_s. \tag{50}$$

On the partially saturated-unsaturated boundary $z = h_3(t)$, the kinematic boundary condition states that the boundary advances with the flow. We also have that the saturation is zero there,

$$\frac{\mathrm{d}h_3}{\mathrm{d}t} = \bar{w}_s, \tag{51}$$

$$S = 0. \tag{52}$$

4.5 Analysis and discussion

(4.5.1)   From Table 1 we have, to leading order in G, the pressure in the droplet is constant and equal to the pressure at the free surface, $p \equiv p_{\text{top}}$. The pressure in the Darcy region is then given by

$$\bar{p}_d = p_{\text{top}} \left(1 - \frac{z}{h_2(t)} \right), \tag{53}$$

where the fact that $j(S = 1) = 0$ has been used, i.e., there is no capillary pressure at the top of the partially-saturated region. Using this expression, the velocity in the Darcy region can be found and this velocity is, in fact, equal to the velocity of the fluid in the droplet via (36). In particular,

$$w \equiv \bar{w}_d = p_{\text{top}}/h_2(t). \tag{54}$$

This solution can be used to construct an expression for the thickness of the droplet, namely

$$h_1(t) = 1 + \phi p_{\text{top}} \int_0^t \frac{\mathrm{d}\xi}{h_2(\xi)} - \frac{T_{\text{sat}}}{T_{\text{evap}}} t. \tag{55}$$

However, to close this expression, a functional form for h_2 must be obtained.

(4.5.2)   From these expressions it can be seen that the pressure gradient that exists between the droplet and the bottom of the Darcy region is due solely to the pressure at the drop of the droplet, p_{top}. Thus, if this pressure vanishes then there is nothing to drive liquid from the droplet into the porous medium and the Darcy region cannot grow. Furthermore, if a fully-saturated Darcy region does not exist initially and if there is no additional pressure at the top of the droplet, then this Darcy region is not likely to come into existence at all. This is a significant result since we postulated the creation of a third region was dependent on an impact force which is effectively p_{top}. Therefore, if $p_{\text{top}} = 0$ then the above two-zone model will provide an adequate mathematical description of the situation. In what follows below we will assume that p_{top} is not equal to zero so that the Darcy region does exist.

(4.5.3) The remainder of the problem amounts to obtaining expressions for the saturation S in the partially-saturated region and determining the boundaries of the regions, h_2 and h_3. This can, in principle, be obtained by seeking a similarity solution to the problem in the partially-saturated region. That is, we write $\eta = z/h_2(t)$ so that $S(z,t) = f(\eta)$, and moreover, we let $h_3(t) = \lambda h_2(t)$ for some λ that must be determined. For the system to be similar it follows that $h_2(t) = -\sqrt{2\Lambda t}$ where Λ is given by

$$\Lambda = p_{\text{top}} + D(1)f'(1), \tag{56}$$

with the prime denoting differentiation with respect to η. Note that this implies that $h_3(t) \propto t^{1/2}$, which is identical to what is found in the two-zone model.

(4.5.4) Under this similarity transformation, Richards' equation becomes

$$\Lambda \eta f' + (D(f)f')' = 0 \tag{57}$$

subject to the conditions $f(1) = 1$ and $f(\lambda) = 0$, where the constant λ is given implicitly by

$$\lambda \Lambda = -D(0)f'(\lambda) \tag{58}$$

via (51). Note that although $D(0) = 0$, we expect $f'(\lambda) \to -\infty$ in such a way that the product of these two values is equal to a finite and nonzero value. Moreover, by integrating (57) over the domain and using integration by parts, this expression can be replaced by

$$\lambda = \frac{p_{\text{top}}}{\Lambda} - 2 - \int_1^\lambda f(\eta) \, d\eta, \tag{59}$$

which is more advantageous to use when solving this problem numerically. Having determined λ and hence Λ, we would have a closed expression for the evolution of the droplet,

$$h_1(t) = 1 - \phi p_{\text{top}} \sqrt{\frac{2t}{\Lambda}} - \frac{T_{\text{sat}}}{T_{\text{evap}}} t. \tag{60}$$

Table 2: Numerically computed values of Λ and λ for different values of p_{top} when the diffusivity is given by (43).

| p_{top}	Λ	λ
1/3	4.52×10^{-2}	3.38
1/2	8.29×10^{-2}	2.65
1	2.12×10^{-1}	1.88
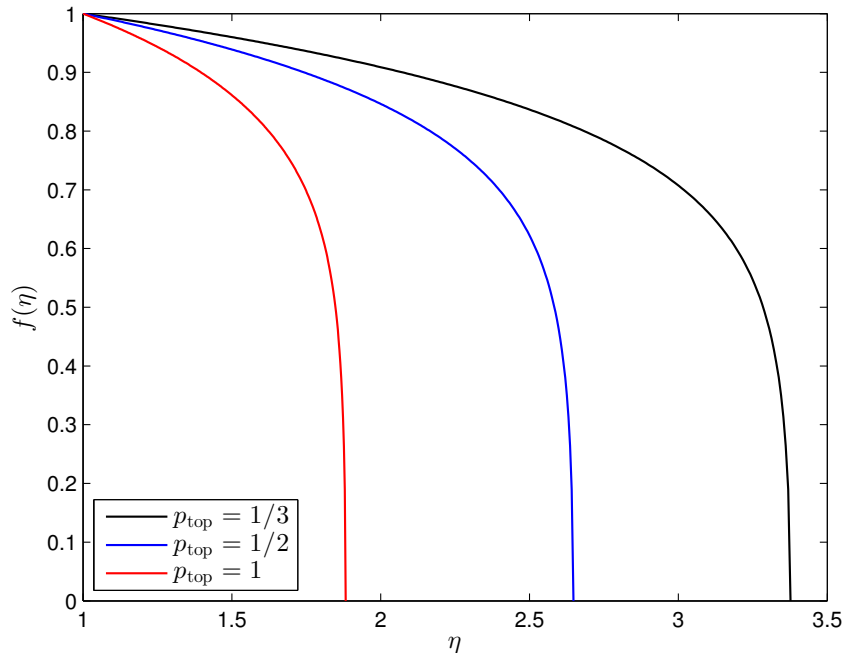
Figure 11: Saturation profiles for different values of p_{top} and for the diffusivity given in (43). See text for details of the calculation.

(4.5.5)   Obtaining analytical expressions for the remaining quantities was not possible so numerical methods were used to approximate them. In particular, Richards' equation (57) was discretized using finite differences and solved in conjunction with (56) and (59). The diffusivity given in (43) was used in the computations. The results for different values of p_{top} can be found in Table 2 and in Figure 11. The results indicate that as p_{top} increases, the growth rate of the fully-saturated region increases, while the growth rate and the width of the partially-saturated region decreases.

5   Evaporation of droplets in a porous media

5.1   Evaporation from the surface

(5.1.1)   Once the drop is fully absorbed in the porous medium the saturation S at the surface will begin to decrease as the fluid spreads through the medium. We model the effect of evaporation at this surface by assuming that there is a flux q_{evap} of fluid out of the medium that is proportional to the local saturation $S(0, t)$,

$$- D_0 D(S) \frac{\partial S}{\partial z} = q_{\text{evap}} = -ES \quad \text{at } z = 0.$$

(5.1.2)   The saturation S satisfies Richards' equation as in section 3, and again we take $D(S) = (n/2)S^n[1 - S^n/(n + 1)]$. One-dimensional numerical

solutions of this equation at a given time for different evaporation rates E are shown in figure 12. This figure shows that evaporative loss from the surface acts both to reduce the volume of fluid in the porous medium and to slow the rate at which the saturation front advances. Thus, enhancing the evaporation rate at the surface can act to limit the volume of porous medium that is contaminated by fluid. We should note that evaporation is a complex process, which is critically dependent on ambient conditions: thus the observations made here give only a qualitative description of the effect of evaporation.
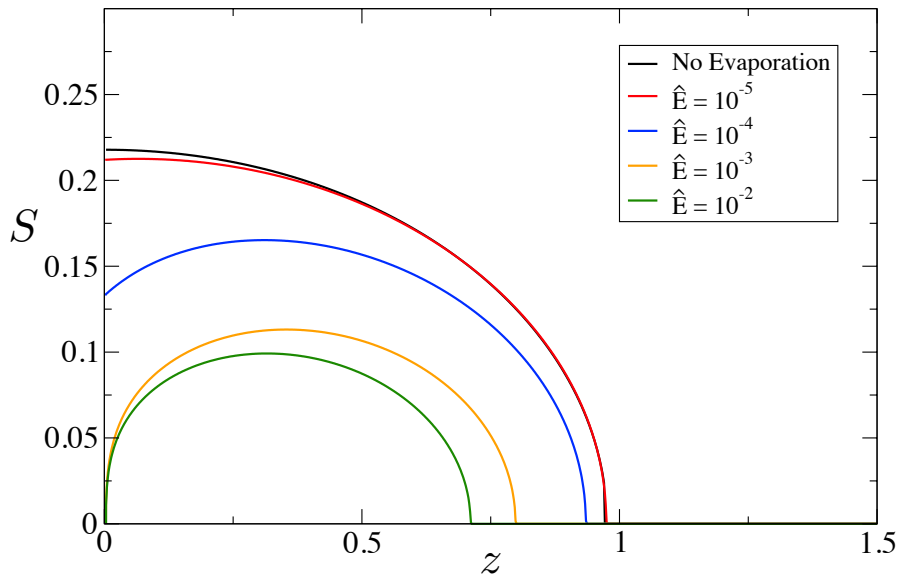

Figure 12: Numerical solutions of Richards' equation for $n = 2$ after the drop has been fully absorbed, showing the effects of evaporation from the surface $z = 0$ for different values of the scaled evaporation rate $\hat{E} = E/D_0$ after time $t = 5\phi/D_0$.

5.2 A tentative model for evaporation from the bulk

(5.2.1) In addition to the evaporation through the surface of the porous medium, in regions of partial saturation, the liquid can evaporate adding to the gaseous phase at each point within the porous medium. To model this effect, in addition to considering the evolution of the liquid within the porous media, we must also consider the behaviour of the gas phase that occupies the remainder of the pore space. Consequently equations governing the vapour density ρ_g must also be given to model this effect, as well as equations for the degree of saturation s.

(5.2.2) At the top boundary $z = 0$, liquid can still evaporate through the surface of the porous media (as in the previous section), and again the evaporation

of liquid through the surface corresponds to a flux with the form

$$-D(S)\frac{\partial S}{\partial z} = -\hat{E}S. \tag{61}$$

At the surface of the porous media, if gas phase is free to mix with a much larger rapidly circulating body of gas in the atmosphere which is otherwise free of vapourized chemical weapons agents, then we can take $\rho_g = 0$.

(5.2.3)   In the partially saturated region $-H < z < 0$, the conservation of liquid and vapour are given by

$$\phi\frac{\partial S}{\partial t} = \frac{\partial}{\partial z}\left[D(S)\frac{\partial S}{\partial z}\right] - \frac{\dot{m}}{\rho_l}, \tag{62a}$$

$$\phi\frac{\partial}{\partial t}\left[(1-S)\rho_g\right] = \frac{\partial}{\partial z}\left[(1-S)D_g\frac{\partial \rho_g}{\partial z}\right] + \dot{m}, \tag{62b}$$

respectively, where the sink term $\dot{m}$, in the liquid conservation equation represents the rate of evaporation of liquid, with an equivalent source term contributing to the vapour phase. One possible way of modelling the rate of evaporation is to assume that it is proportional to the difference between the concentration of vapour in the gas ρ_g, and the concentration of vapour in the gas at saturation $\rho_{g,sat}$.

(5.2.4)   At the bottom of the partial saturation fringe at $z = -H$, the degree the saturation $S = 0$, while the vapour density is continuous across the limit of liquid infiltration.

(5.2.5)   In the dry region $z < -H$, there is no liquid present so $S = 0$. However the liquid vapour is still able to diffuse into this region driven by the vapour concentration gradient. This can be modelled by a conservation law for the mass of vapour with the form

$$\phi\frac{\partial}{\partial t}\left[(1-s)\rho_g\right] = \frac{\partial}{\partial z}\left[D_g\frac{\partial \rho_g}{\partial z}\right]. \tag{63}$$

(5.2.6)   During the study group there was insufficient time to investigate liquid evaporation within the partially saturated region any further. Additional theoretical work is required to model the evaporation of a droplet within a porous media and details of how this modelling could be approached are given by Kaviany (1995) [15] and Bear and Bachmat (1990) [3].

6   Conclusions

6.1   Conclusions

(6.1.1)   Droplet impacts onto porous media are complicated phenomena, which are not fully understood. Depending on the parameters associated with

a falling droplet and the substrate it impacts, a wide range of different behaviours are possible, including splashing, spreading across the substrate, impact pressure driven droplet infiltration, capillary driven droplet infiltration and finally liquid evaporation. These processes occur across a range of different time scales and this fact can be used to analyse the different phases of a droplet impact and subsequent absorption.

(6.1.2) The initial behaviour of a liquid droplet that hits a porous media in a droplet impact is very different to the behaviour of a liquid droplet that is gently placed upon the surface of the porous media. In an impact, the pressure generated in the liquid that results from the rapid deceleration of a droplet as it hits a porous substrate is expected to generate a region just below the impact site of the porous medium, whose pore spaces are almost completely saturated by liquid from the droplet. The equivalent fully saturated region beneath a droplet placed upon the surface of the porous media is expect to be smaller, as initially only surface tension exists to drive liquid into the pore spaces. Over longer time scales, the liquid in the porous media is expected to gradually diffuse away from the initial impact site, although the degree of saturation will fall as the distance from the impact site increases.

(6.1.3) Evaporation of liquid can occur from *(i)* the droplet free-surface, *(ii)* the surface of a saturated porous medium and *(iii)* the bulk of a partially saturated porous medium. Liquid evaporation from the surface of a droplet sitting on the surface of a porous media is particularly important for relatively impermeable materials such as concrete, where the initial absorption of the droplet is comparatively slow. However, it is much less relevant for droplets impacting sand, where the initial absorption is much more rapid. Over a longer time (after the droplet has been absorbed), liquid can evaporate from the surface of the porous media and also within partially saturated regions within the porous media. Liquid evaporation slows the spreading of liquid through the pore spaces as less liquid is available. Further investigation into models of liquid evaporation are required, particularly in regions of partial saturation.

(6.1.4) Further experiments are needed, particularly in relation to the onset of splashing and to capture the evolution of the liquid within the porous media. High-speed photography of droplet impacts with a range of substrates with surface roughness and porous materials would be particularly valuable in understanding the initial droplet behaviour. In the first instance these experiments could be conducted safely using water as its liquid properties are close enough to the chemical weapons agents of interest to further understanding of these complicated phenomena.

6.2 Recommendations for future numerical investigation of droplet impacts and infiltration into porous media

(6.2.1)   DSTL are interested in large scale numerical simulations of droplet impact with porous media. As an example of a possible approach they wish to investigate, DSTL cited Reis *et al.* [24], who investigate the spreading and infiltration of droplet impacts with porous media using the method of marker particles. DSTL have also used a volume of fluid method to perform their own preliminary investigations of these phenomena.

(6.2.2)   Over the course of the week the study group was unable to perform their own simulations of the full droplet impact problem. However, members of the group have previously investigated a range of different problems associated with droplet impacts using the volume of fluid method. The study group noted that simulations of droplet impact with porous media in the literature [24, 23] and conducted by DSTL, assumed a passive gas phase within the simulation. This is equivalent of modelling the droplet impact within a vacuum and under these assumptions, the liquid jets that run along the surface of the substrate never lift off to trigger splashing and the formation of micro-droplets. Liquid jets that run along the surface of the body match experimental results of droplet impact conducted in a vacuum [27], and further suggests that a non-passive gas phase is an important factor in generating splashing.

(6.2.3)   The study group recommends that if DSTL wish to investigate the possibility of splashing (in addition to spreading and infiltration), within their simulations of droplet impact, then a model with an active gas phase should be used. Historically interface capturing numerical schemes such as the volume of fluid method have been more successful at modelling a liquid within a passive gas phase, while with an active gas phase, they have tended to struggle if the difference between the initial gas and liquid density is as large as that associated with air and water. This explains the prominence of a passive gas phase in simulations of droplet impact. Given the liquids that are of interest to DSTL, density differences equivalent to those seen with air and water are to be expected (see §A.1). However, recent use of more advanced linear solvers used in such schemes have enabled accurate front capturing volume of fluid methods to be developed for cases with high density ratios. Such schemes are present within the Gerris Flow solver [21] and OpenFOAM [9].

(6.2.4)   Using a volume of fluid method it is difficult to model partial saturation of the porous media, as a volume of fluid method is designed to capture the interface to a region that is fully saturated. DSTL have experimented with using volume of fluid methods within a porous media, by explicitly modelling the liquid infiltration into each individual pore space. DSTL make this calculation with using an idealized porous media, whose pore

spaces are the volumes separating an array of packed spheres. An example of such a porous media and a snapshot of the fluid infiltrating through it is shown in figure 13. Explicit calculations such as this are enormously computationally expensive, and while the voids between packed spheres may represent some porous media, the behaviour of liquids in many materials (for instance materials with anisotropic porosity and permeability), will be poorly represented by such an approach.
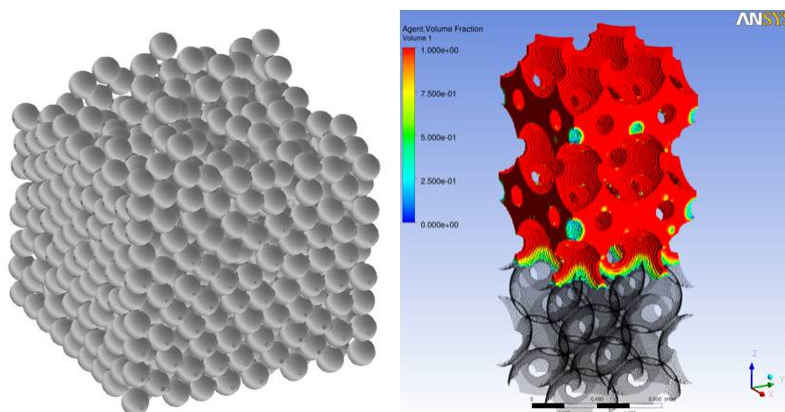

Figure 13: Existing DSTL simulations of liquid infiltration into a porous medium.

(6.2.5) The study group envisages an alternative approach where only the initial touchdown, spreading and impact pressure driven infiltration phase is captured using a volume of fluid method. After this initial phase the subsequent capillary suction driven phase of the liquid infiltration would be modelled using Richards' equation. This would calculate the average degree of saturation across a local collection of pore spaces, rather than the explicit position of the liquid interface within each pore space. Together with a library of hydraulic conductivities for a range of different porous media, this can provide higher fidelity to the expected liquid behaviour (compared to an array of packed spheres), at a massively reduced computational cost.

(6.2.6) Although the study group focussed primarily on one-dimensional models of capillary suction driven liquid infiltration, the extension of Richards' equation to three-spatial dimensions is easily achieved. In three spatial dimensions more complicated models for the droplet behaviour on the surface are required. However, models based upon the thin film equations could be profitably be used here and could readily incorporate features such the pressure generated by surface tension and the droplet interface curvature. The development of such models is significantly aided by experimental results of droplets infiltrating into sand, which show that the position of the contact line between droplet, porous medium and air does not change over time, while the contact angle decreases to allow the vol-

ume of the liquid in the droplet to fall [7]. While beyond the scope of the study group, coupled models based on the thin film equations for the droplet behaviour above the porous media and Richards' equation for the saturation evolution within the porous media, would be comparatively easy to develop and should provide a fruitful technique for future investigations of droplet infiltration into porous media.

A   Appendix

A.1   Properties of chemical weapons agents

Table 3: Properties of chemical weapons agents. Values obtained from Augerson (2000) [2].

Property	Symbol	Sarin	Sulphur Mustard	VX	Units
Density	ρ	1102	1270	1012.4	$\mathrm{kg\,m^{-3}}$
Viscosity	μ	0.00139	0.005175	0.0123	$\mathrm{Pa\,s}$
Surface tension	σ	0.026	0.042	0.032	$\mathrm{Pa\,m^{-1}}$

A.2   Properties of porous media

Table 4: Representative values for the properties of porous media. Values obtained from Navaz *et al.* (2008) [19].

Substrate	Porosity ϕ	Permeability K (m^2)
High-silica, medium-grain sand	0.44	6.05×10^{-11}
Fine sand	0.37	2.30×10^{-12}
Glass beads	0.28	4.80×10^{-13}
Ceramic tile	0.26	5.00×10^{-14}
Concrete	0.25	$5 - 30 \times 10^{-15}$

Bibliography

[1] N. Alleborn and H. Raszillier. Spreading and sorption of a droplet on a porous substrate. *Chem. Eng. Sci.*, 59(10):2071–2088, May 2004, doi: 10.1016/j.ces.2004.02.006.

[2] W. Augerson. *A Review of the Scientific Literature as it Pertains to Gulf War Illnesses, Volume 5: Chemical and Biological Warfare Agents*, chapter Appendix B: Data on nerve agents, pages 195–205. RAND Corporation, 2000.

[3] J. Bear and Y. Bachmat. *Introduction to modeling of transport phenomena in porous media*, volume 4 of *Theory and Applications of Transport in Porous Media*. Springer, 1990.

[4] L. Bridge, R. Bradean, M. J. Ward, and Wetton B. R. The analysis of a two-phase zone with condensation in a porous medium. *J. Eng. Math.*, 45:247–268, 2003, doi: 10.1023/A:1022690802938.

[5] A. T. Corey. The interrelation between gas and oil relative permeabilities. *Producers Monthly*, 19(1):38–41, 1954.

[6] S. H. Davis and L. M. Hocking. Spreading and imbibition of viscous liquid on a porous base. II. *Phys. Fluids*, 12(7):1646–1655, 2000, doi: 10.1063/1.870416.

[7] T. G. D'Onofrio, H. K. Navaz, B. Markicevic, B. A. Mantooth, and Sumpter K. B. Experimental and Numerical Study of Spread and Sorption of VX Sessile Droplets into Medium Grain-Size Sand. *Langmuir*, 26(22):3317–3322, 2010, doi: 10.1021/la903071q.

[8] A. S. Ellis, F. T. Smith, and A. H. White. Droplet impact onto a rough surface. *Q. J. Mech. Appl. Math.*, 64(2):107–139, 2011, doi: 10.1093/qjmam/hbq026.

[9] OpenFOAM Foundation. `http://www.openfoam.org`, 2010.

[10] H. Giesche. Mercury porosimetry: A general (practical) overview. *Part. Part. Syst. Char.*, 23(1):9–19, 2006, doi: 10.1002/ppsc.200601009.

[11] S. D. Howison, J. R. Ockendon, J. M. Oliver, R. Purvis, and F. T. Smith. Droplet impact on a thin fluid layer. *J. Fluid Mech.*, 542:1–23, 2005, doi: 10.1017/S0022112005006282.

[12] S. D. Howison, J. R. Ockendon, and S. K. Wilson. Incompressible water-entry problems at small deadrise angles. *J. Fluid Mech.*, 222:215–230, 1991, doi: 10.1017/S0022112091001076.

[13] A. Iafrati and A. A. Korobkin. Self-similar solutions for porous/perforated wedge entry problem. In *Proceedings of the 20th International Workshop on Water Waves and Floating Bodies, Longyearbyen, Norway*, 2005.

[14] C. Josserand, L. Lemoyne, R. Troeger, and S. Zaleski. Droplet impact on a dry surface: triggering the splash with a small obstacle. *J. Fluid Mech.*, 524:47–56, 2005, doi: 10.1017/S0022112004002393.

[15] M. Kaviany. *Principles of Heat Transfer in Porous Media*. Mechanical Engineering Series. Springer, 2nd edition, 1995.

[16] J. O. Marston, S. T. Thoroddsen, W. K. Ng, and R. B. H. Tan. Experimental study of liquid drop impact onto a powder surface. *Powder Tech.*, 203(2):223–236, 2010, doi: 10.1016/j.powtec.2010.05.012.

[17] B. Molin and A. A. Korobkin. Water entry of a perforated wedge. In K. Mori and H. Iwashita, editors, *Proceedings of the 16th International Workshop on Water Waves and Floating Bodies, Hiroshima, Japan*, 2001.

[18] C. Mundo, M. Sommerfeld, and C. Tropea. Droplet-wall collisions: experimental studies of the deformation and breakup process. *Int. J. Multiphase Flow*, 21:151, 1995, doi: 10.1016/0301-9322(94)00069-V.

[19] H. K. Navaz, B. Markicevic, A. R. Zand, Y. Sikorski, E. Chan, M. Sanders, and T. G. D'Onofrio. Sessile droplet spread into porous substrates–determination of capillary pressure using a continuum approach. *J. Colloid Interface Sci.*, 325(2):440–6, September 2008, doi: 10.1016/j.jcis.2008.04.078.

[20] J. M. Oliver. *Water entry and related problems.* PhD thesis, University of Oxford, Oxford, United Kingdom, 2002.

[21] S. Popinet. Gerris flow solver. `http://gfs.sourceforge.net`, 2012.

[22] R. Purvis and F. T. Smith. Droplet impact on water layers: post-impact analysis and computations. *Phil. Trans. R. Soc. Lond. A*, 363:1209–1221, April 2005, doi: 10.1098/rsta.2005.1562.

[23] N. C. Reis, R. F. Griffiths, and J. M. Santos. Numerical simulation of the impact of liquid droplets on porous surfaces. *J. Comp. Phys.*, 198(2):747–770, 2004, doi: 10.1016/j.jcp.2004.01.024.

[24] N. C. Reis, R. F. Griffiths, and J. M. Santos. Parametric study of liquid droplets impinging on porous surfaces. *Appl. Math. Model.*, 32(3):341–361, 2008, doi: 10.1016/j.apm.2006.12.006.

[25] L. A. Richards. Capillary conduction of liquids through porous mediums. *Physics*, 1(5):318–333, 1931, doi: 10.1063/1.1745010.

[26] T. P. Witelski. Perturbation analysis for wetting fronts in Richards' equation. *Transport Porous Med.*, 27(1):121–134, 1997, doi: 10.1023/A:1006513009125.

[27] L. Xu, W. W. Zhang, and S. R. Nagel. Drop splashing on a dry smooth surface. *Phys. Rev. Lett.*, 94:184505, 2005, doi: 10.1103/PhysRevLett.94.184505.